Journal of Atomic, Molecular, Condensate & Nano Physics
Vol. 1, No. 2, pp. 87–97, 2014
ISSN 2349-2716 (online); 2349-6088 (print)
Published by RGN Publications

http://www.rgnpublications.com

Nonlinear Refractive Index of Silicon Nanoparticles: A Short Review

Review Article

Sudakshina Prusty

School of Physical Sciences, National Institute of Science Education and Research (NISER), Sachivalaya Marg, PO Sainik School, Bhubaneswar, Orissa 751005, India
sprusty@niser.ac.in

Abstract. This article discusses the nonlinear refractive index of silicon nanoparticles starting from the basic formalism to some of the consequent physical phenomena like self focusing and self phase modulation. Several experimental techniques mainly based on Z-scan are discussed to measure the nonlinear refractive index. Another less explored technique for silicon nanoparticles, which studies the far-field optical fringe pattern formed by spatial self-phase modulation, is also discussed. Computation of the nonlinear refractive index is shown in detail by employing these two techniques. While Z-scan can estimate the nonlinear coefficient of a medium in a chosen time scale, the optical fringe method can predict the overall nonlinear refractive index due to all possible physical mechanisms. Some of the recent results for silicon nanoparticles using these two techniques are also discussed.

Keywords. Nonlinear refractive index; Self focussing; Self-phase modulation; Silicon nanoparticles; Z-scan technique; Optical fringe

PACS. 68.35.Md

Received: February 7, 2014 **Accepted:** May 21, 2014

Copyright © 2014 Sudakshina Prusty. *This is an open access article distributed under the Creative Commons Attribution License, which permits unrestricted use, distribution, and reproduction in any medium, provided the original work is properly cited.*

1. Introduction

Nonlinear optical properties of materials have become increasingly important since the invention of laser. The origin of nonlinear (NL) optics lies in the NL response of materials to the incident laser radiation. Potentially, NL optical effects can play a major role in the development of high-speed data-processing and communication systems. Various all-optical NL devices operating as switches, routers or frequency converters, have been shown to be technically feasible, but they are not yet of practical interest because of the limitations of existing NL materials.

In the past decades, silicon nanoparticles (SiNP) have generated large interest as a promising key material to establish a Si based photonics [1]. Room temperature light emission from SiNP is attainable by reducing their dimensions down to a few nanometers, localizing the electron-hole pairs. On the other hand, the low absorption coefficient makes SiNP attractive as active medium in waveguide structures. In recent years, tremendous research work has been undertaken to explore the NL optical properties of low dimensional semiconductors, especially, SiNP [2–11]. Optical nonlinearities of the SiNP are relatively larger than that in bulk Si and about 200 times larger than that for silica at fiber-optic wavelengths [1], making this system a good candidate for applications in nonlinear optics. It has been shown that there is a strong correlation of the third-order optical nonlinearity and hence the NL refractive index, of the SiNP with the electronic quantum confinement effect [11, 12]. Recently, an all-optical logic gate operating in the gigabits per second regime exploiting the NL optical properties of SiNP is demonstrated [13], as both the absorption coefficient and refractive index can be easily controlled by the application of external optical fluences.

This article is organised as follows: Section 2 gives a formal theoretical background of NL refractive index, its origin and discusses some fascinating NL phenomena like self focussing and self-phase modulation. Section 3 discusses some of the experimental techniques to measure the NL refractive index of NL media in various forms. In Section 4 computation of NL refractive index is shown in detail by employing two techniques in particular, e.g. Z scan and optical fringe pattern formation. Some of the recent results for SiNP using these two techniques are also discussed.

2. Theoretical Background

In this section, let us recall some concepts of NL optics. Let $P(\omega)$ be the induced polarization in a medium at a given frequency ω due to an electric field $E(\omega)$ of an incident laser radiation. At low laser intensities, one can assume that $P(\omega)$ depends linearly on $E(\omega)$. Neglecting anisotropy, the linear optical properties of a given material at frequency ω are fully described by the refractive index $n(\omega)$ or the relative dielectric constant $\varepsilon_r(\omega)$ or the susceptibility $\chi(\omega)$. Since the ω dependence of the above mentioned quantities is obvious, henceforth it will be dropped from the notations for simplicity. The relation among these quantities are given by $\varepsilon_r = n^2 = 1 + \chi$. At sufficiently high laser intensities, P deviates from its linear dependence on E. The expression for P involves higher-order terms in E. In electric dipole approximation, P can be mathematically expressed in a Taylor series as

$$P = \varepsilon_0[\chi^{(1)}E + \chi^{(2)}EE + \chi^{(3)}EEE + \ldots] \tag{1}$$

where ε_0, $\chi^{(n)}$ and $\boldsymbol{E}$ are the dielectric permittivity of free space, the nth order susceptibility tensor and the electric field in the medium respectively. This expression is valid only if the optical frequency is non-resonant and $\boldsymbol{E}$ is not too large so that the series expansion converges rapidly. These susceptibilities are solely the properties of the material and depend upon the electronic structure of the atoms/molecules as well as their geometrical arrangement in the bulk. For example, $\chi^{(2)}$ vanishes for materials with inversion symmetry. The first term on the right hand side of Eq. (1) denotes the linear polarization, which varies linearly with electric field $\boldsymbol{E}$. This is responsible for linear absorption and refraction. The remaining terms are associated with light-induced NL effects. The second term $\chi^{(2)}\boldsymbol{EE}$ has a quadratic dependence on the electric field $\boldsymbol{E}$. This second-order polarization gives rise to the electro-optic effect,

second harmonic generation, sum frequency generation and other second-order processes. The third-order polarization denoted by $\chi^{(3)}\boldsymbol{EEE}$ is responsible for third harmonic generation, optical phase conjugation and intensity dependent absorption and refraction in the medium. All the above NL optical phenomena are exploited in developing various devices for frequency conversion, optical switching, optical limiting and optical logic circuits, etc.

Since the susceptibility is a function of $\boldsymbol{E}$, the refractive index, n, of the medium depends on $\boldsymbol{E}$. For a NL medium, this dependence has significant contribution when subjected to intense electromagnetic field leading to an effect called self focusing. Since this does not affect the frequency, one can extract the expression for refractive index from Eq. (1) by choosing the fundamental harmonic term as follows [14]

$$n = \sqrt{1 + \left(\chi^{(1)} + \frac{3}{4}\chi^{(3)}|E|^2\right)}\,. \tag{2}$$

This can further be simply expressed as the combination of linear and NL contributions

$$n = n_0 + \Delta n(|E|^2) \tag{3}$$

where n_0 is the intensity independent linear refractive index and $\Delta n(|E|^2)$, the intensity dependent NL refractive index induced by an optical field E.

The NL refractive index is determined by several physical mechanisms acting on a broad range of time scales. The various contributions are

$$n_{nl} = n_{nl}(\text{electronic}) + n_{nl}(\text{non-electronic})\,. \tag{4}$$

The electronic contribution originates from optical transitions involving the bound electrons having very fast response time, of the order of 10^{-15}s. The non-electronic processes are nonradiative interactions due to vibrational, electrostrictive and thermal contributions. The vibrational response time is of the order of 10^{-13}s[15]. The electrostrictive response time is roughly equal to the time required for an acoustic deformation to travel across the diameter of the beam ($\sim 10^{-8}$s). Thermal diffusion time scales are even longer and depend on the thermal properties of the medium. Examples of electronic nonlinearity are second- and third harmonic generation. Some of non-electronic NL phenomenon are temperature-, density-, and order parameter-changes, cis-trans isomerism, phase transition, etc.

Now let us discuss the effects of NL refractive index of a medium in form of some physical processes. When an intense beam passes through a medium having refractive index given by Eq. (3), it yields to some very fascinating phenomena like self focusing and self phase modulation [16]. These are typical of NL wave propagation that results from wavefront distortions inflicted on a beam by itself while traversing a NL medium. Consider a single mode laser beam with a Gaussian transverse profile propagating into the said medium with a refractive index n. If Δn is positive, the central part of the Gaussian beam having a higher intensity should experience a larger refractive index while traversing the medium. Therefore, beam travels at a slower velocity than that at the edge. Consequently, the original plane wavefront of the beam gets progressively more curved, when the beam travels in the medium [16]. The distortion is similar to that imposed on the beam by a positive lens. Since the optical ray propagation is in the direction perpendicular to the wavefront, the beam appears to focus by itself. Thus, self-focusing can be briefly explained as an induced lens effect. If Δn is negative, a negative lens effect occurs giving rise to a similar reverse phenomenon, known as self defocusing.

However, the beam should undergo diffraction due to its finite cross-section. Self-focusing will be prominent only when it is stronger than diffraction. In many cases, the field-induced refractive index of a NL medium can be approximated by

$$\Delta n = \left\{\frac{n_2}{2}|E|^2\right\}_{esu} = \{n_2 I\}_{MKS} \tag{5}$$

where n_2 is a constant, called as the NL coefficient and I is the intensity of the incident beam (in MKS). Since $|E|$ (in CGS units) is inversely proportional to the beam radius, the self-focusing action remains stronger than the diffraction action (if it was strong initially, otherwise the latter will dominate).

The change in optical-field-induced refractive index also leads to self-induced phase modulation of the beam. Consider a laser pulse $|E(t)|^2$ propagating in a NL medium of length l. If Δn in the medium has an instantaneous response $\Delta n(t) = \frac{n_2}{2}|E(t)|^2$, the output has a self-phase modulation given by [16]

$$\Delta\phi(t) = \frac{\omega}{c}\Delta n(t) l = \frac{\omega}{c}\frac{n_2}{2}|E(t)|^2 l \tag{6}$$

Correspondingly this results in a frequency modulation, $\Delta\omega(t) = -\frac{\partial(\Delta\phi(t))}{\partial t}$, which appears to be a broadened spectrum.

Analogically, a similar phenomenon of self-phase modulation can occur in space depending on the transverse intensity profile of a beam, which is known as spatial self-phase modulation. When an intense laser beam passes through a NL medium, the change in the refractive index gives rise to a velocity distribution of the laser beam in the transverse plane. Hence there occurs spatial phase variation. For a beam with a Gaussian-like transverse profile, the phase increment $\Delta\phi(r)$ across the beam profile has a bell-shaped distribution and can be written as [16]

$$\Delta\phi(r) = \Delta\phi_0 \exp\left(\frac{-2r^2}{a^2}\right) \tag{7}$$

where a is a constant and $\Delta\phi_0$ is the maximum phase increment at $r = 0$. Thus constructive or destructive interference occur when $\Delta\phi(r_1) - \Delta\phi(r_2) = m\pi$, for m being an even or odd integer respectively. When $\Delta\phi_0$ is much larger than 2π, a concentric multiple ring pattern appears on the far-field observation screen placed perpendicular to the direction of the transmitted beam through the NL medium. The total number of rings, N, can be estimated from the relation [16]

$$N \cong \frac{\Delta\phi_0}{2\pi}. \tag{8}$$

Concentric optical fringe patterns due to self-phase modulation have been observed in various systems such as, SiNP [17], Gold nanoparticles [18, 19] and nematic liquid crystal films [20] using a continuous wave laser beam.

3. Experimental Techniques

The NL refractive index can be measured by using a variety of techniques including NL interferometry [21], degenerate four-wave mixing [22], nearly degenerate three-wave mixing [23], ellipse rotation [24] and beam distortion measurements [25]. The first three methods, namely, NL interferometry and wave mixing, are potentially sensitive techniques,

but require relatively complex experimental apparatus. On the other hand, beam distortion measurements are relatively insensitive and require detailed wave propagation analysis. A very simple and sensitive single-beam technique, termed as Z-scan technique, has been demonstrated by Sheik-Bahae *et al*. [26] in order to measure both the sign and magnitude of the NL refractive index and NL absorption coefficient for a wide variety of materials in different time scales. In case of SiNP, Z-scan is the extensively used technique to estimate the NL coefficient as discussed in the next section. This technique in particular and some other specific techniques are discussed in the following.

(i) Z-scan

In the conventional Z-scan experiment, the transmittance of a NL medium is recorded by a photodetector while the sample (which is a NL medium) is scanned through (Z-axis) the focused laser beam. This is called an open aperture Z-scan. Plot between sample position (z) measured with respect to the focal plane and the normalized transmittance curve depicts only the losses due to the linear and NL absorptions of the sample from which the NL absorption coefficient is calculated. If the transmitted light is measured through a finite aperture in the far field as a function of the sample position, it is called as a closed aperture Z-scan. The curve displays both the absorption and scattering where the coefficient of NL refractive index can be obtained. A general scheme of the setup of the Z-scan technique is depicted in Fig. 1. As the sample moves through the beam focus (at $z = 0$), self-focusing or -defocusing modifies the wave front phase, thereby modifying the detected beam intensity. A pre-focal transmittance maximum (peak), followed by a post-focal transmittance minimum (valley) is a Z-scan signature of a *negative nonlinearity*. An inverse Z-scan curve (i.e., a valley followed by a peak) characterize a *positive nonlinearity*. Fig. 2 depicts these two situations.

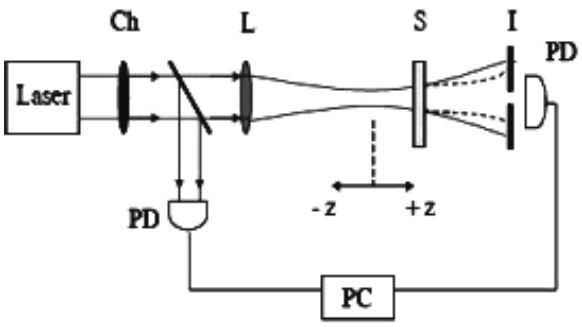

Figure 1. General schematics of experimental setup of the Z-scan technique: chopper (Ch); lens (L); sample (S); iris (I), photo detector (PD) and personal computer (PC).

(ii) Modified forms of Z-scan

Since its invention, the conventional Z scan technique has been improvised for better sensitivity and to study a variety of materials. These include the use of non-Gaussian-beam profiles, thick samples, measurements in reflection mode (reflection Z-scan, appropriate for opaque materials) and total beam-profile distortions [27]. In spite of these advances, however, it is still not convenient to use the Z-scan technique in certain situations. For example, the excitation laser wavelength has to be off resonance for strongly NL absorption materials so that transmitted optical signal can be measured. Weak NL materials require intense optical beam, often resulting

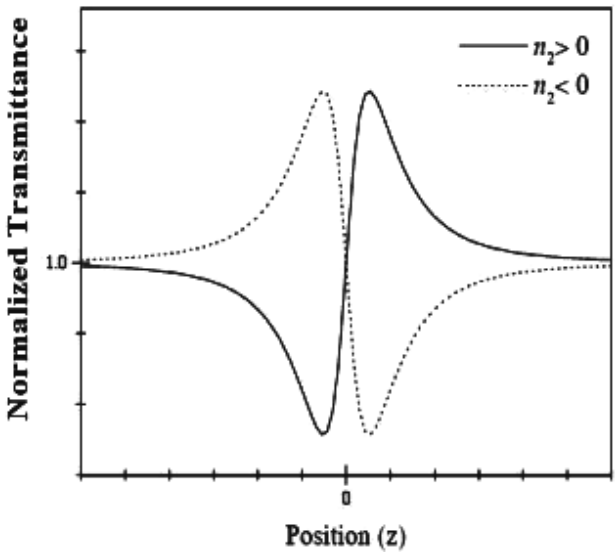

Figure 2. Typical Z-scan plots showing positive and negative nonlinearity.

in damage of the material. Also Z-scan cannot be used to study opaque and highly absorptive optical samples, and surface properties of non-transparent materials like semiconductors. This holds true even for frozen aqueous samples where formation of microcrystals and cracks lowers the transparency of the sample.

There is a novel Photoacoustic Z scan (PAZ scan) [27] technique devised recently to measure the NL absorption coefficient of a wide variety of non-transparent, highly absorbing, optically thick samples. This technique combines the advantages of the conventional Z scan method and the sensitivity of photoacoustic detection. In this method the sample is scanned through the focused laser beam and the generated photoacoustic signal is recorded using a focused ultrasound transducer.

The NL response of a material can have several physical origins and it is important to differentiate among them. As for example, when some glassy materials or liquids are excited by a continuous (cw) or quasi-cw (with high repetition rate) laser beam, thermal nonlinearities are unavoidable. In that case, a thermally managed eclipse Z scan technique [28] is used to simultaneously measure the thermal and non-thermal contribution to the NL refractive properties along with the absorptive properties.

(iii) Optical fringe pattern

Another potential technique, but little explored for SiNP, is the formation of optical fringe pattern. With this technique, the NL refractive index is calculated by studying the optical fringe pattern formed due to spatial self phase modulation of a focused cw laser beam after traversing through a NL medium [17–20]. Since the fringe pattern can be observed in reflection geometry, this method is also useful to measure the change in refractive index of an opaque medium e.g. semiconductors. However, it is not possible to know the exact physical origin of nonlinearity by this method as the fringe pattern is related to the total change in refractive index due to all possible NL processes.

4. Discussions

This section deals with calculation and discussion of some results of nonlinear refractive index using Z-scan and optical fringe pattern methods. The Z-scan method has been used extensively by many research groups to measure the third-order NL susceptibility [4–6] and the NL refractive index [7–11] resulting from the quantum confinement of Si. In this technique, to calculate the nonlinear coefficient, the experimentally measured closed aperture transmittance $T(x)$ is fitted with the following expression [29]

$$T(x) = 1 + \frac{4\Delta\phi}{(x^2+9)(x^2+1)}. \tag{9}$$

where $x = z/z_0$, is defined as the reduced distance from the focal point, z being the absolute longitudinal distance and z_0 the Rayleigh range of the beam and $\Delta\Phi$ is the phase change. This phase change $\Delta\Phi$ is related to the nonlinear coefficient n_2 (in SI units) by

$$n_2 = \Delta\phi\lambda\alpha/[2\sqrt{2}\pi I_0(1-e^{-\alpha l})] \tag{10}$$

where α, I_0 and l are the linear absorption coefficient at the used wavelength λ, the peak intensity at the focus position and the thickness of the sample, respectively.

The NL coefficient of the refractive index has been calculated at different wavelengths (or excitation energies) for SiNP prepared by various fabrication methods. Hernandez *et al*. [29] have evaluated the NL coefficient for SiNPs prepared by plasma enhanced chemical vapor deposition. For excitation at 0.80 eV, in the nanosecond regime, the nonlinearity is mainly of thermal origin and the NL coefficient is very high, -10^{-8}cm^2/W. For excitation at 1.5 eV, in the femtosecond regime, the nonlinearity is due to electronic response and the NL coefficient is smaller, 10^{-12}cm^2/W. The electronic susceptibility, associated with intraband transitions, is highly enhanced for SiNP with a size below 2 nm due to the appearance of electronic transitions between discrete levels induced by quantum confinement. Changing the pulse duration in nanosecond range increases the NL coefficient proportionately as shown for SiNP embedded in SiO_2 films at 1.16 eV [30]. In this regime, it is shown that free carriers hold major influence on the NL properties as compared to two-photon absorption (TPA), bound electron or thermal effects. In another report [31], the NL coefficient of a similar system (SiNP in SiO_2 films) is shown to be large in the excitation range 1.52 to 1.66 eV, due to contribution from defect states at low annealing temperatures. As the crystals grow with higher annealing temperature, the defect state contribution is reduced and the quantized electronic states are considered to be the major origin of the large NL coefficient. References [32] and [33] show some methods to enhance the NL coefficient further in a confined system. SiNP doped with phosphorus (P) show enhanced NL coefficient as P concentration increased at 1.6 eV in the femtosecond range [32]. This is a strong indication that impurity control may be an additional parameter to enhance the NL optical responses of SiNP. Petris *et al*. [33] measured precisely both electronic and thermal NL coefficients of periodic nano-patterned Si on insulator (SOI), un-patterned SOI and bulk silicon, using a reflection Z-scan setup with femtosecond laser pulses at 1.55 eV. These results could be important in silicon photonics, for achievement of NL optical devices with properties controlled by nano-patterning. Most of the data reported so far show large deviations due to the inhomogeneity of the samples owing to various fabrication techniques, preparation conditions and different particle size distributions.

There are several reports [17–20, 34] on computation of NL refractive index by studying the optical fringe patterns formed by far-field diffraction from various NL media. Consider a

Gaussian laser beam of the following intensity profile, $I(r)$, is incident on a NL medium.

$$I(r) = I_0 \exp\left(-\frac{2r^2}{\omega^2}\right) \tag{11}$$

where I_0 the maximum intensity at the center of the Gaussian laser beam and ω is the beam waist. The far-field diffraction intensity distribution from such a medium is given by [20]

$$I(x) = I_0 \left| i\left(\frac{2\pi}{\lambda Z}\right)\int_0^\infty r dr J_0\left(\frac{krx}{2Z}\right)\exp\left(-2\frac{r^2}{\omega^2} - i\phi(r)\right)\right|^2 \tag{12}$$

where x is the distance from the center of the far field pattern to the observation point, λ the wavelength of incident laser beam, z the distance from the sample to the observation point, $J_0(x)$ the zero-order Bessel function of the first kind and k $(= 2\pi/\lambda)$ the wave number in free space. The phase shift $\phi(r)$ plays the most important role in determining the final intensity distribution. It consists of two parts contributed by the linear and NL phase differences. The linear part is due to the distance Z and the radius of curvature R of the wavefront of the incident laser beam. The nonlinear part of phase shift is given by

$$\phi_{Nl}(r) = k \ln_2 I(r). \tag{13}$$

There are several physical mechanisms which can induce a change in refractive index proportional to the light intensity in a NL medium. According to Eq. (12), the far-field diffraction patterns will be alike as long as the additional phase shifts are identical. In other words, the effect of the additional phase shift caused by the refractive index change on the far-field diffraction pattern is only relevant to the magnitude of the additional phase shift produced after the beam passes through the medium. It is not relevant to the mechanism by which the change in the refractive index occurs. By simulation of the experimental far-field intensity distribution pattern by using Eqs. (12) and (13), the NL coefficient can be estimated. The value of n_2 can also be estimated by a simple linear relation between the number rings and the maximum nonlinear phase shift $\phi_{Nl}(0)$ using Eqs. (8) and (13), of course with proper attention paid to the beam curvature R [18].

Though this method is well studied in materials like liquid crystals [20], surprisingly there are very few reports of application of this method to nanoparticles [17–19]. The NL refractive index is measured by Prusty *et al*. [17] for SiNP prepared by laser-induced etching. Here they show that the NL coefficient depends on the size distribution of the nanoparticles present in the medium. Thus, the optical fringe pattern formed at the far-field in reflection geometry evolves not only with the incident laser intensity, but also with the change in size distribution. Fig. 3 shows the far-field intensity distribution of optical fringe patterns calculated theoretically. Fig. 3(a) corresponds to the pattern formed by the probing laser beam of intensity 0.3 kW/cm^2, when it falls on a bulk Si substrate where the SiNP are not yet formed. An intensity distribution is shown to evolve in Fig. 3(b) as SiNP are formed with an average size of 4 nm, when probed at an intensity of 0.3 kW/cm^2. As the probing intensity is increased from 0.3 and 0.6 kW/cm^2 keeping the size constant, the far-field intensity distribution evolves further as shown in Fig. 3(c). Figs. 4(a)-(c) are the experimentally observed fringe patterns corresponding, respectively, to Figs. 3(a)-(c). Thus the overall change in refractive index contributing to the nonlinear phase shift is shown to be a function of the particle sizes and the probing beam intensity. Since

the sample is kept in the focal plane, the linear part of the phase shift only gives a constant contribution.

Majles Ara *et al*. [19] have shown a fair agreement between the estimated values of the NL coefficient of gold nanoparticles by comparing the results of Z-scan and optical fringe pattern method. The interplay between the number of generated rings and the nonlinear phase-shift induced by convergent and divergent Gaussian beams is thoroughly investigated theoretically and experimentally for a colloidal solution of gold nanoparticles [18]. By looking to the whole changes in the diffraction patterns, they show that a linear relation exists for both situations. The effect of contributions from both the linear and NL phase differences on the formation and evolution of the far-field diffraction pattern of a Gaussian beam passing through nonlinear media is studied in detail by numerical method [34]. When the divergent Gaussian beam passes through the self-defocusing media, or the convergent Gaussian beam passes through the self-focusing media, the thick diffraction ring pattern with both the central dark spot and the larger distribution range will emerge in the far-field plane. Whereas in reverse case, when a divergent Gaussian beam transmits through the self-focusing media, or the convergent Gaussian beam passes through the self-defocusing media, the thin diffraction ring pattern with both the central bright spot and the smaller distribution range will emerge in the far-field plane. However, extreme care must be exercised while using this simple linear relation to estimate the NL coefficient experimentally since the total phase difference also depends on the sign and value of the beam curvature at the sample position.

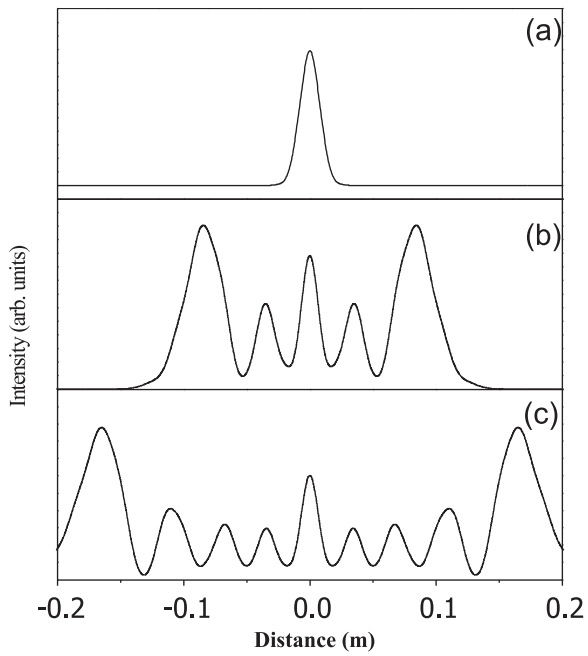

Figure 3. Theoretically calculated far-field intensity distribution of optical fringe patterns (a) in absence of SiNP at a probing laser beam of intensity 0.3 kW/cm^2, (b) in presence of SiNP of average size of 4 nm at a probing laser beam of intensity 0.3 kW/cm^2 and (c) in presence of SiNP of average size of 4 nm at a probing laser beam of intensity 0.6 kW/cm^2.

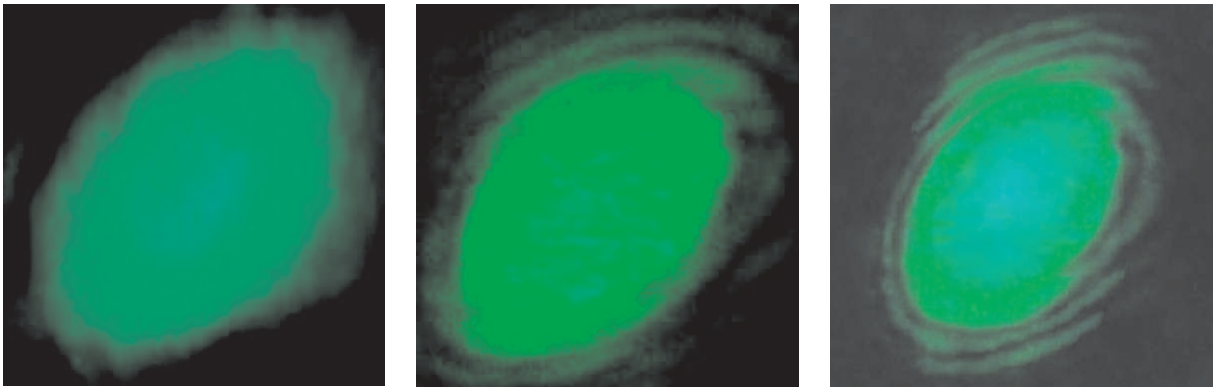

(a) (b) (c)

Figure 4. (a)-(c): Experimentally observed fringe patterns corresponding, respectively, to the calculated far-field intensity distribution shown in Figs 3(a)-(c).

5. Conclusions

In summary, the NL refractive index of the SiNP is discussed starting from the basic formalism to some of the consequent physical phenomena like self focusing and self phase modulation. Among various available experimental techniques, the Z scan method is invariably used to estimate the NL coefficient for SiNP, prepared under various fabrication conditions, subjected to various time scales and different excitation energies. This leads to a large scatter in the available data. Estimation of NL refractive index from the far-field optical fringe pattern of SiNP is also discussed in detail. With careful analysis of the fringe pattern, one can estimate the overall NL refractive index due to all possible physical mechanisms in the SiNP. It also predicts that apart from the incident laser intensity, NL coefficient is dependent on the size distribution of SiNP.

Competing Interests

The author declare that they have no competing interests.

Authors' Contributions

Author contributed significantly in writing this article. The author read and approved the final manuscript.

References

[1] N. Daldosso and L. Pavesi, Nanosilicon, edited by Vijay Kumar (Elsevier, New York, 2005), Chapter 1.

[2] R. Chen, D.L. Lin and B. Mendoza, Phys. Rev. B **48**, 11879 (1993).

[3] P. Maly, J. Kudrna, F. Trojanek and A. Hospodkova, Thin Solid Films **276**, 84 (1996).

[4] F.Z. Henari, K. Morgenstern, W.J. Blau, V.A. Karavanskii and V.S. Dneprovskii, Appl. Phys. Lett. **67**, 323 (1995).

[5] S. Vijayalakshmi, M.A. George and H. Grebel, Appl. Phys. Lett. **70**, 708 (1997).

[6] G. Vijayaprakash, M. Cazzanelli, Z. Gaburro, L. Pavesi, F. Iacona, G. Franzo and F. Priolo, J. Appl. Phys. **91** 4607, (2002).

[7] M. Takahashi, Y. Toriumi, T. Matsumoto, Y. Masumoto and N. Koshida, Appl. Phys. Lett. **76** 1990, (2000).

[8] S. Lettieri, O. Fiore, P. Maddalena, D. Ninno, G.D. Francia, V. La Ferrara, Opt. Commun. **168** 383, (1999).

[9] S. Lettieri, O. Fiore, P. Maddalena, A. Morra and D. Ninno, Philosphical Mag. B **81** 133, (2001).

[10] S. Vijayalakshmi, H. Grebel, G. Yaglioglu, R. Pino, R. Dorsinville and C.W. White, J. Appl. Phys. **88** 6418, (2000).

[11] S. Vijayalakshmi, M.A. George and H. Grebel, Appl. Phys. Lett. **70**, 708 (1997).

[12] D. Cotter, M.G. Burt and R.J. Manning, Phys. Rev. Lett. **68**, 1200 (1992).

[13] Demonstration of an all-optical logic gate, within the European Project Phologic (Contract HP6-017158), based on the nonlinear optical response of Si-nc.

[14] B.B. Laud, Lasers and Nonlinear Optics, New Age International, India, 173 (1991).

[15] R. Adair, L.L. Chase and S.A. Payne, Phys. Rev. B, **39**, 3337 (1989).

[16] Y.R. Shen, The Principles of Nonlinear Optics, John Wiley & Sons, New York, 303 (1984).

[17] S. Prusty, H.S. Mavi and A.K. Shukla, Phy. Rev. B **71**, 113313 (2005).

[18] C.M. Nascimento, M.A.R.C. Alencar, S. Chavez-Cerda, M.G.A. da Silva, M.R. Meneghetti and J.M. Hickmann, J. Opt. A: Pure Appl. Opt. **8**, 947 (2006).

[19] M.H. MajlesAra, Z. Dehghani, R. Sahraei, A. Daneshfar, Z. Javadi and F. Divsar, Journal of Quantitative Spectroscopy & Radiative Transfer **113**, 366 (2012).

[20] H. Ono, Y. Harato, Jpn. J. Appl. Phys. **37**, 4061 (1998).

[21] M.J. Moran, C.Y. She and R.L. Carman, IEEE J. Quantum Electron. **11**, 259 (1975).

[22] S.R. Friberg and P.W. Smith, IEEE J. Quantum Electron. **23**, 2089 (1987).

[23] R. Adair, L.L. Chase and S.A. Payne, J. Opt. Soc. Am. B, **4**, 875 (1987).

[24] A. Owyoung, IEEE J. Quantum Electron. **9**, 1064 (1973).

[25] W.E. Williams, M.J. Soileau and E.W. Van-Stryland, Opt. Commun. **50**, 256 (1984).

[26] M. Sheik-Bahae, A.A. Said, T. Wei, D.J. Hagan and E.W. Van-Stryland, IEEE J. Quantum Electron. **26**, 760 (1990).

[27] C.S. Yelleswarapu and S.R. Kothapalli, Optics Express **18**, 9020 (2010).

[28] A.S.L. Gomes, E.L. Falcao Filho and Cid B. de Araújo, Diego Rativa and R.E. de Araujo, Optics Express **15**, 1712 (2007).

[29] S. Hernandez, P. Pellegrino, A. Martinez, Y. Lebour, B. Garrido, R. Spano, M. Cazzanelli, N. Daldosso, L. Pavesi, E. Jordana and J.M. Fedeli, J. App. Phy. **103**, 064309 (2008).

[30] A. Martinez, S. Hernandez, P. Pellegrino, O. Jambois, B. Garrido, E. Jordana and J.M. Fedeli, J. App. Phy. **108**, 014311 (2010).

[31] M. Ito, K. Imakita, M. Fujii and S. Hayashi, J. Appl. Phys. **108**, 063512 (2010).

[32] M. Ito, K. Imakita, M. Fujii and S. Hayashi, J. Phys. D: Appl. Phys. **43**, 505101 (2010).

[33] A. Petris, F. Pettazzi, E. Fazio, 1378;
C. Peroz, Y. Chen, V.I. Vlad and M. Bertolotti, J. Optoelectronics & Advanced Materials **8**, 1377 (2006).

[34] L. Deng, K. He, T. Zhou and C. Li, J. Opt. A: Pure Appl. Opt. **7** 409, (2005).